THE JOURNAL OF PHYSICAL CHEMISTRY C

Article

Cite This: J. Phys. Chem. C 2018, 122, 21991−21997

pubs.acs.org/JPCC

Ab Initio Predictions of Double-Layer TiO_2-Terminated $SrTiO_3$(001) Surface Reconstructions

Seyoung Cook and Laurence D. Marks*

Department of Materials Science and Engineering, Northwestern University, Evanston, Illinois 60208, United States

Supporting Information

ABSTRACT: Predicting oxide surface structures, and surface structures in general, is a significant science frontier. Herein, we demonstrate an Ising model approach combined with density-functional calculations to predict several $SrTiO_3$(001) surface reconstructions. Constrained Ising tilings of $TiO_5\square$ truncated octahedral units are used to construct the TiO_2 adlayers of $SrTiO_3$(001) surface reconstructions with TiO_2 double-layer terminations for a given periodicity and composition. This method is used to re-examine the $(\sqrt{5} \times \sqrt{5})R26.6°$ reconstruction and to predict several $(\sqrt{10} \times \sqrt{10})R18.4°$ reconstructions. The surface structures and energies of the newly predicted reconstructions, along with consideration of the previously reported $(\sqrt{13} \times \sqrt{13})R33.7°$, 3×3, and $(\sqrt{2} \times \sqrt{2})R45.0°$ reconstructions, indicate that the larger, more complex TiO_2 double-layer $SrTiO_3$(001) reconstructions with lower coverages of the TiO_2 adlayer are made up of recurrent structural motifs represented by smaller, simpler reconstructions with higher coverages of the TiO_2 adlayer. These results demonstrate a route forward for predicting oxide and other surface structures using a relatively simple computational approach.

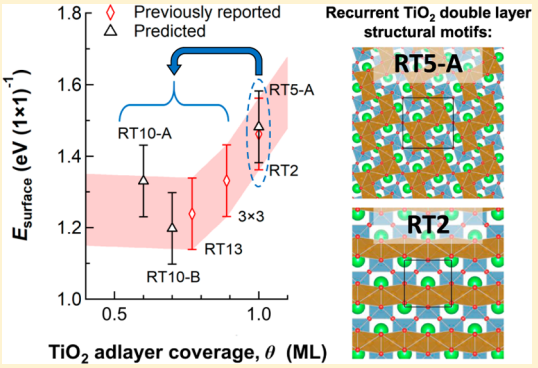

I. INTRODUCTION

The (001) surface of strontium titanate ($SrTiO_3$ or STO) is technologically important in the burgeoning field of oxide electronics[1,2] as it is widely used as a structural template for the growth of epitaxial oxide thin films and heterostructures featuring a two-dimensional (2D) electron gas.[3,4] Understanding the surface structure of this prototypical perovskite oxide is thus relevant, and well-ordered reconstructed STO(001) surfaces are beginning to be explored for their potential applications in the areas of thin-film growth,[5−8] epitaxy of nanoparticles,[9,10] and catalysis.[11−13] One of the key challenges is in understanding in a general fashion, ideally with predictive power, the structures of these reconstructed surfaces, given that the structure, symmetry, composition, and even the cation co-ordination of a reconstruction differ substantially from the bulk. Numerous reconstructions have been observed on the (001) surface of STO, including 1×1,[14−17] 2×1,[14,16−20] 2×2,[15,16,21−24] $(\sqrt{5} \times \sqrt{5})R26.6°$,[22,25−29] $c(4 \times 2)$,[20,30,31] $c(4 \times 4)$,[16,22,31−33] 4×4,[22] $(\sqrt{13} \times \sqrt{13})R33.7°$,[18,34] and $c(6 \times 2)$.[18,30,31,35−37] These reconstructions are ubiquitous in that they form under a variety of experimental conditions and synthesis methods, appearing in single-crystal samples annealed in oxygen[19,20,24,34,37] or vacuum,[17,31,38,39] in thin films grown by hybrid molecular beam epitaxy,[40,41] and in hydrothermally synthesized nanocuboids.[42,43]

The atomic structures of many of the STO(001) surface reconstructions have been solved,[19,20,24,34,37] and these surfaces are known to be Ti-rich. The Ti-rich composition arises as typical surface preparation methods for STO(001) involve etching away the surface strontium by a chemical means, followed by annealing in an oxidizing environment to produce atomically flat surfaces.[44−48] There are many factors that determine which particular reconstruction is stabilized in the end, as it is strongly history-dependent and in some cases influenced by surface hydrolysis[49] and dissociative adsorption of water.[32,50] A 1×1 surface is typically observed, which in many cases is likely locally disordered.[51]

Regarding the Ti co-ordination at the surface, many of the solved reconstructions[19,20,24,34] are based on a TiO_2 double layer (DL) with units of TiO_6 or $TiO_5\square$ ($\square$ a vacant site). This is illustrated using the $(\sqrt{13} \times \sqrt{13})R33.7°$ (RT13) reconstruction in Figure 1a. A TiO_2-DL STO(001) reconstruction can be regarded as a TiO_2 adlayer consisting of corner- and edge-sharing network of truncated $TiO_5\square$ octahedral units, meshed on top of a bulk-like TiO_2 base layer.[34] There are two basic structural features regarding the bonding of the Ti atom in the adlayer with O atoms necessary to form the network of $TiO_5\square$ truncated octahedra, which we will collectively refer to as Ti−O bonding requirements: (1) each Ti atom in the adlayer must be bonded to an O atom in the TiO_2 base layer and (2) each O atom in the adlayer must be bonded to two or more Ti atoms. This suggests that by enforcing these constraints on the chemical bonding, together

Received: July 24, 2018
Revised: August 30, 2018
Published: September 4, 2018

DOI: 10.1021/acs.jpcc.8b07128
J. Phys. Chem. C 2018, 122, 21991−21997

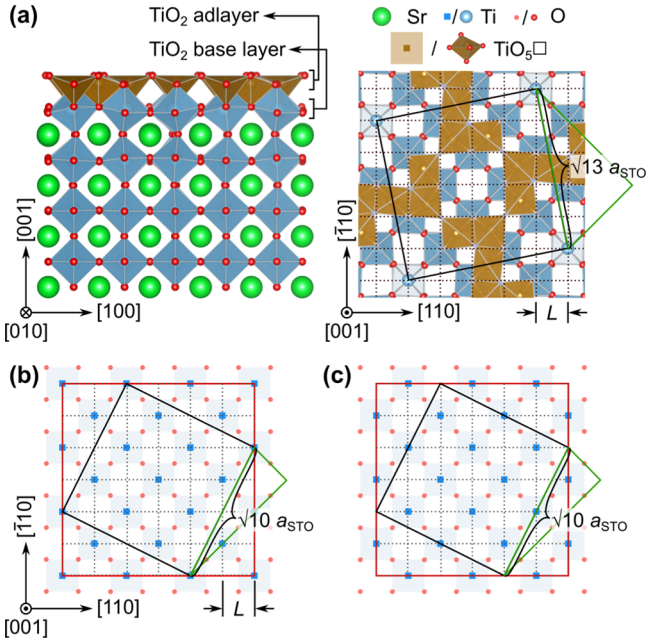

Figure 1. Building a TiO_2 double-layer (DL) $SrTiO_3(001)$ surface structure based on a TiO_2 adlayer with constrained Ising tilings of $TiO_5\square$ units on a TiO_2 base layer. (a) Left: profile view of the $(\sqrt{13} \times \sqrt{13})R33.7°$ (RT13) reconstruction showing the TiO_2-DL surface termination. Right: plan view of the RT13 surface overlaid with a grid of square cells, each outlining a site that can be occupied by a $TiO_5\square$ truncated octahedral unit in the adlayer. Here, top-most oxygen atoms are removed for clarity. (b, c) Physically allowed tilings of the $TiO_5\square$ units classified according to the vertices of the bounding square (red) circumscribing the 2D unit cell of the reconstruction, centered on Ti sites and oxygen 4-fold hollow (OFH) sites in the TiO_2 base layer, respectively, illustrated for the $(\sqrt{10} \times \sqrt{10})R18.4°$ reconstruction. L is the square edge length of $TiO_5\square$. Strontium atoms are removed in the plan view illustrations for clarity.

with relaxation of atomic positions based on density functional theory (DFT), we can generate TiO_2-DL STO(001) surface reconstructions with locally satisfied bond valence sums (BVSs)[52] of arbitrary periodicity and composition, and they will be low-energy structures. If this is possible, it would constitute a major step forward in prediction of oxide surface structures.

In this work, we demonstrate that a fairly simple Ising model approach can successfully produce new, low-energy surface structures. We enumerate $(\sqrt{10} \times \sqrt{10})R18.4°$ (RT10) and $(\sqrt{5} \times \sqrt{5})R26.6°$ (RT5) TiO_2-DL STO(001) reconstructions constructed by tiling $TiO_5\square$ units in the TiO_2 adlayer and use density-functional calculations to predict low-energy RT10 and RT5 reconstructions. First, RT10 and RT5 reconstructions are enumerated that satisfy the two basic Ti−O bonding requirements found in known TiO_2-DL STO(001) reconstructions. Next, atomic positions of possible reconstructions are relaxed using density-functional calculations. Low-energy reconstructions are identified by comparing their calculated surface energies against those of known STO(001) reconstructions using a convex-hull construction across different surface compositions. In examining the atomic structures of the newly predicted and previously reported TiO_2-DL STO(001) reconstructions along the convex hull, we find recurrent structural motifs represented by the smaller reconstructions, RT5 and $(\sqrt{2} \times \sqrt{2})R45.0°$ (RT2), which have full coverages of the TiO_2 adlayer. We discuss the implications of these recurrent structural motifs and those of adsorbate interactions on real STO(001) surfaces, as well as the general applicability of our computational approach to other surfaces beyond just oxides, which can open the door to substantial new science.

II. COMPUTATIONAL METHODS

II.I. Enumeration of TiO_2 Double-Layer Structures. Computationally, the TiO_2 adlayer in a TiO_2-DL STO(001) reconstruction can be modeled by a set of discrete $TiO_5\square$ units occupying a grid set by the square 2D lattice of O atoms in the TiO_2 base layer, which represents a constrained Ising tiling. This is illustrated in Figure 1a for the RT13 reconstruction, where the grid is subdivided in units of $TiO_5\square$ edge length (L) to represent sites that can be occupied by a $TiO_5\square$ unit (gold square), centered on an O atom (red dot) in the TiO_2 base layer. A convenient way to construct a reconstruction is by defining a "bounding square", which circumscribes the 2D unit cell of the adlayer and the overall reconstruction, classified according to the sites within the TiO_2 base layer on which its vertices are centered. Figure 1b,c shows the physically allowed bounding square configurations, with vertices centered on Ti sites and oxygen 4-fold hollow (OFH) sites, respectively, for the RT10 reconstruction. Similar bounding square with vertices centered on the O sites results in unphysical Ti−Ti or Ti−OFH site bonding (Figure S1). We note that these configurations can be generalized to differently sized reconstructions (e.g., the RT5 reconstruction in our study). With these physically allowed TiO_2 base layer configurations, we can satisfy the first structural requirement that each Ti atom in the adlayer is bonded to an O atom in the TiO_2 base layer, simply by filling in the grid of allowed $TiO_5\square$ sites to form the TiO_2 adlayer. The next step is to generate all possible adlayer configurations and check that each O atom in the adlayer is bonded to two or more Ti atoms.

Figure 2 outlines the flow of the algorithm used to enumerate possible TiO_2-DL STO(001) reconstructions. A given reconstruction sets the size of the bounding square in the

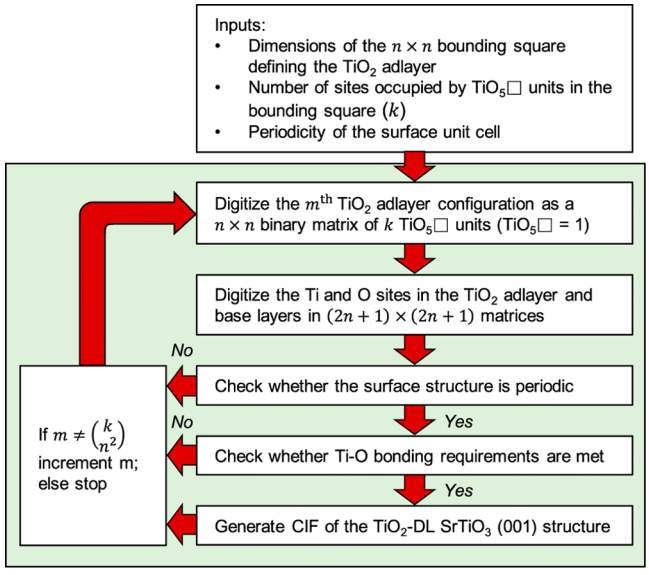

Figure 2. Flow diagram of the algorithm used to enumerate TiO_2 double-layer $SrTiO_3(001)$ surface reconstructions.

DOI: 10.1021/acs.jpcc.8b07128
J. Phys. Chem. C 2018, 122, 21991−21997

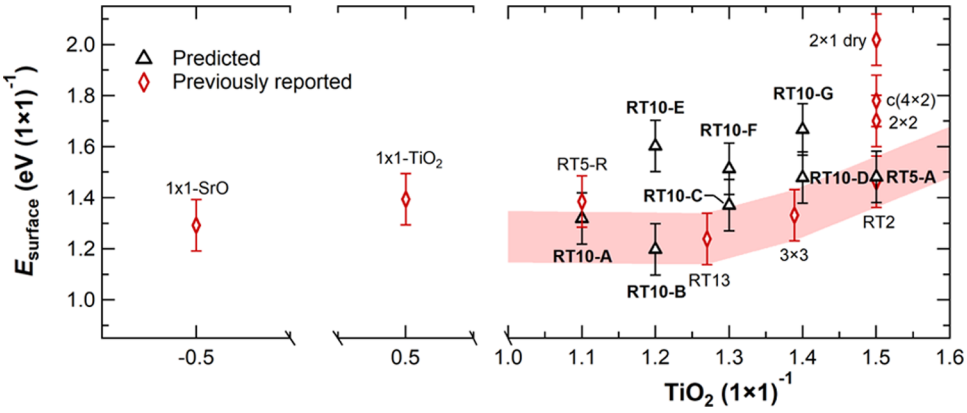

Figure 3. Surface energies in eV $(1 \times 1\ \text{cell})^{-1}$ versus TiO_2 $(1 \times 1\ \text{cell})^{-1}$ for various $SrTiO_3(001)$ reconstructions, including DFT error estimate of ± 0.1 eV $(1 \times 1\ \text{cell})^{-1}$. The shaded region represents a section of the convex-hull construction taken from ref 37. TiO_2 $(1 \times 1)^{-1}$ (0.5) corresponds to single-layer TiO_2 surface termination and 1.5 TiO_2 $(1 \times 1)^{-1}$ corresponds to double-layer TiO_2 surface termination with a full coverage of the TiO_2 adlayer.

TiO_2 adlayer ($n \times n$ grid) as well as the 2D unit cell, where the n^2 sites can be occupied by k $TiO_5\square$ units. For a given occupation k/n^2 of the adlayer, n^2 choose k configurations are possible. In this algorithm, each of the n^2 choose k configurations is generated, starting with a binary number that is then wrapped around into a $n \times n$ matrix. The $n \times n$ matrix is then expanded to a $(2n + 1) \times (2n + 1)$ matrix to include explicitly the occupied Ti and O sites. Similar matrices are generated for the underlying TiO_2 base layers. Each adlayer configuration is first tested for translational symmetry. If translation symmetry exists, then the configuration is tested to make sure each O atom in the adlayer is bonded to two or more Ti atoms. Once these criteria are met, the binary configuration is saved along with a tag for the 2D unit cell and the TiO_2 base layer configuration. From this information, the crystallographic information file for the TiO_2-DL STO(001) structure is generated, and the space group is determined. Surfaces with $p1$ symmetry are physically unlikely to form extended repeat units and were thus excluded from subsequent density-functional calculations. Details of the RT10 and RT5 TiO_2-DL structure generation are provided in the Supporting Information.

II.II. Density Functional Calculations. Ab initio density-functional calculations were carried out using the (linearized augmented plane wave) (L)APW+lo method as implemented in the `WIEN2K` code.[53] Atomic positions were optimized using the modified Perdew–Burke–Ernzerhof functional (PBEsol)[54] implementation of the generalized gradient approximation. For each surface structure considered, a three-dimensional periodic surface slab model was created consisting of seven layers of the STO bulk plus two TiO_2 surface layers separated by 12 Å of vacuum, with inversion symmetry. The in-plane lattice parameter was based on the DFT-optimized bulk lattice parameter of STO (3.901 Å), using the muffin-tin radii (R_{MT}s) of 1.90, 1.53, and 1.35 Bohrs for Sr, Ti, and O, respectively. These R_{MT}s were used in relaxing the atomic positions until the force per atom, energy, and charge converged to within 0.1 eV/Å, 0.01 eV, and 0.005e, respectively. The largest reciprocal lattice vector K_{max} used in the plane-wave expansion was given by $R_{MT}^{min}K_{max} = 5.5$, where R_{MT}^{min} is the smallest muffin-tin radius, and a k-mesh consisting of one k-point in the irreducible wedge of the first Brillouin zone was used when relaxing the atomic positions.

In calculating the final surface energies, the revTPSSh method[55] was used with an exact-exchange parameter of 0.5 for the Ti-d levels, which was previously determined using experimental energies of several TiO_x molecules.[34] In these calculations, R_{MT}s of 2.33, 1.72, and 1.55 Bohr were used for Sr, Ti, and O, respectively, and a $R_{MT}^{min}K_{max}$ value of 7.0 was used. A k-point sampling equivalent to $6 \times 6 \times 1$ for the 1×1 single-layer TiO_2/SrO surface structures was used across different structures to keep the same reciprocal space sampling density. Energies of several known STO(001) surfaces were also calculated for comparison using the same parameters. The surface energy per 1×1 unit cell of each structure was calculated according to

$$E_{surface} = \frac{E_{slab} - E_{STO}N_{STO} - E_{TO}N_{TO}}{2N_{1\times1}} \quad (1)$$

where E_{slab} is the total energy of the slab, E_{STO} is the energy of bulk $SrTiO_3$, N_{STO} is the number of bulk $SrTiO_3$ unit cells, E_{TO} is the energy of bulk rutile TiO_2, N_{TO} is the number of excess TiO_2 units, and $N_{1\times1}$ is the number of 1×1 surface cells. All energies were converged to 0.01 eV $(1 \times 1)^{-1}$, which is below the accuracy of the functional based upon prior tests. To compare the surface energies calculated using the parameters employed in this work with the those in the published works,[34,37] the reference energies of the bulk $SrTiO_3$ and TiO_2 were varied to match the energies for the 1×1-SrO and RT13 surfaces, which span stoichiometries from −0.5 to 1.27 TiO_2 $(1 \times 1)^{-1}$. We note that the energy comparisons were performed based on a convex-hull construction, in which systematic errors in the reference energies only lead to a linear shift of the surface energies and therefore do not affect what structures lie on the convex hull, as discussed later. The surface energies as a function of the surface stoichiometry after applying this correction are presented, with estimated errors of ± 0.1 eV $(1 \times 1)^{-1}$, which were previously determined from consistency check across several different functionals.[37]

III. RESULTS AND DISCUSSION

To make meaningful comparisons of the DFT-computed energies across different compositions and predict new thermodynamically stable reconstructions, we make use of a convex-hull construction. Convex hull is the multidimensional surface connecting the lowest energy structures as a function of

DOI: 10.1021/acs.jpcc.8b07128
J. Phys. Chem. C 2018, 122, 21991−21997

composition and thermodynamic variables,[56,57] here represented as a set of connected straight lines that are each tangent common to the local energy curves of the different STO(001) surfaces. Specifically, the previously determined convex-hull construction in ref 37 connects the 1 × 1-SrO, RT13, 3 × 3, and $c(6 \times 2)$ surfaces, as shown in Figure 3. Any newly predicted surface reconstructions, which are energetically favorable must then fall below or lie on the existing convex hull. A significant advantage of the convex-hull approach is that systematic errors in the energies of the reference (bulk rutile TiO_2 and $SrTiO_3$) lead only to a linear shift of the energies and therefore do not affect what structures lie on the convex hull, i.e., the predicted thermodynamically stable reconstructions.

The computed surface energies per (1 × 1) unit cell and compositions of higher-symmetry (non-$p1$) RT10 and RT5 reconstructions are plotted in Figure 3, along with those of other STO(001) surface reconstructions taken from a previous work.[37] Using the convex hull, we can immediately eliminate several of the candidate RT10 reconstructions (RT10-E, RT10-F, and RT10-G; Figure S2) as these clearly lie above the known convex hull. The differences in the DFT-computed energies of the RT10 reconstructions for a given composition can be rationalized in terms of chemical bonding using structural stability analysis based on BVSs. Here, we define the surface instability index (SII), after the global instability index for bulk structures,[58,59] as the root mean square of the deviation of the BVSs from the expected values for atoms in the surface unit cell (e.g., in the TiO_2 double layer)

$$\mathrm{SII} = \frac{\sqrt{\sum_1^N (\mathrm{BVS} - \mathrm{BVS}_0)^2}}{N} \tag{2}$$

where N is the number of atoms in the unit cell and BVS_0 is the expected BVS, which is the bond valence of an atom in bulk $SrTiO_3$. Smaller SII indicates a higher stability. Our TiO_2-DL structure generation method yields surface structures with generally low SII once the atomic positions are relaxed using density-functional calculations. Across different compositions, the SIIs are not correlated with the surface energies, as shown in Table S1 for the RT10-A, RT13, and RT5-A reconstructions. At a given composition, we find the differences in the DFT-computed energies are consistent with the differences in SIIs, as shown in Tables S2−S4 for the RT10 reconstructions, as expected.

As depicted in Figure 3, we predict several thermodynamically stable RT10 and RT5 reconstructions across different coverages of the TiO_2 adlayer that lie on the previously determined convex hull. Their surface structures are shown in Figure 4a−e. The RT10 reconstructions maintain $p2$ symmetry as the $TiO_5\square$-network structure evolves with increasing monolayer (ML) coverages of the TiO_2 adlayer. The RT10 reconstruction transitions from arrays of kinked-line structures at 0.6 ML adlayer coverage (RT10-A, Figure 4a) to an edge- and corner-sharing $TiO_5\square$ network featuring a fractional hole formed by linking the kinked-line structures seen in RT10-A with a bridging $TiO_5\square$ unit at 0.7 ML adlayer coverage (RT10-B, Figure 4b). Here, an overall translation of the TiO_2 adlayer accommodates bonding of the corner O atoms in the bridging $TiO_5\square$ unit with Ti atoms in the base layer. At 0.8 ML adlayer coverage, a similar kinked-line structure forms as in RT10-A, but with longer linear sections of the edge-sharing $TiO_5\square$ units (RT10-C, Figure 4c). At 0.9 ML adlayer coverage, the structure is significantly different from those

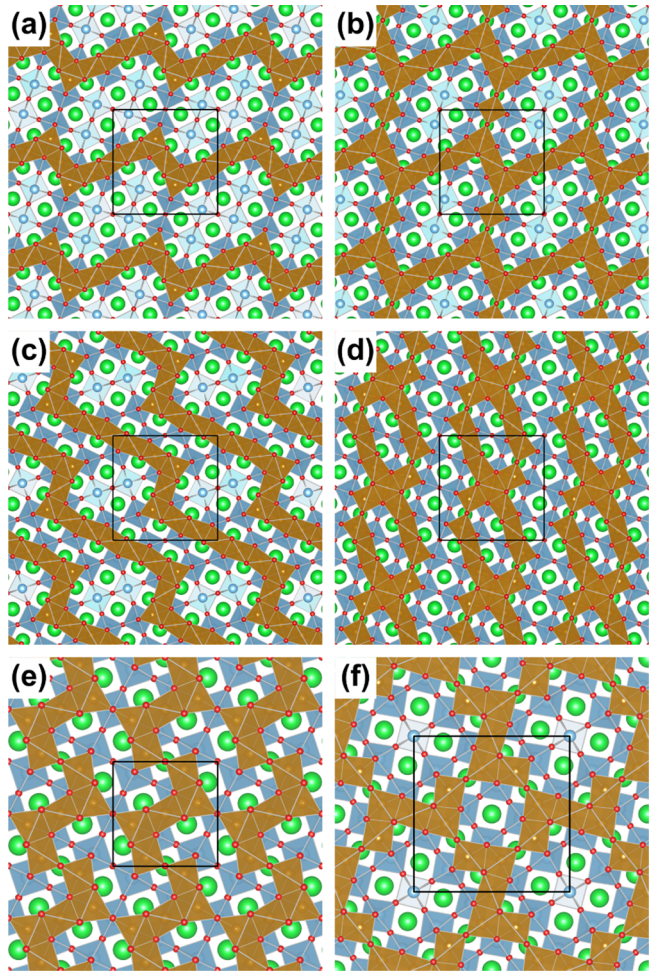

Figure 4. Surface structures of the predicted thermodynamically stable TiO_2 double-layer $SrTiO_3(001)$ $(\sqrt{10} \times \sqrt{10})R18.4°$ (RT10) and $(\sqrt{5} \times \sqrt{5})R26.6°$ (RT5) with different monolayer (ML) coverages of the TiO_2 adlayer. (a) RT10-A (0.6 ML), (b) RT10-B (0.7 ML), (c) RT10-C (0.8 ML), (d) RT10-D (0.9 ML), and (e) RT5-A (1.0 ML) structures. (f) Surface structure of the solved $(\sqrt{13} \times \sqrt{13})R33.7°$ (RT13) reconstruction[34] shown for comparison. Only the two top-most TiO_2 layers and the top-most SrO layers are shown. The kinked-line structural motifs seen in the RT10-A, RT10-B, and RT10-C reconstructions are variations of the structural motif found in the RT5-A reconstruction, which also makes up the RT13 reconstruction.

with lower adlayer coverages, consisting of arrays of elongated cross-shaped motifs (RT10-D, Figure 4d). The predicted RT5 reconstruction (RT5-A, Figure 4e) has a 1.0 ML adlayer coverage and $p2$ symmetry, with a structural motif that is also found in the solved RT13 reconstruction[34] (Figure 4f), but has a lower overall symmetry ($p2$ versus $p4$).

Interestingly, the structural motif in the RT5-A reconstruction is also found in the lower-coverage RT10 reconstructions (RT10-A, RT10-B, and RT10-C). We note that a similar behavior is observed with the previously reported RT2 reconstruction,[23] which has the same surface energy and TiO_2 adlayer coverage as the RT5-A reconstruction (see Figure 3). The structural motif for the RT2 reconstruction is a linear $TiO_5\square$ array, which appears in the 3 × 3 reconstruction[34] found at a lower TiO_2 adlayer coverage (0.89 ML adlayer coverage). These observations indicate that the larger, more complex TiO_2-DL reconstructions with lower coverages of the

DOI: 10.1021/acs.jpcc.8b07128
J. Phys. Chem. C 2018, 122, 21991−21997

TiO_2 adlayer are made up of recurrent structural motifs represented by smaller, simpler reconstructions with higher coverages of the TiO_2 adlayer.

The recurrent structural motifs made up of the $TiO_5\square$ units found in the TiO_2-DL STO(001) reconstructions are consistent with their similar surface energies along the convex hull. As discussed for STO(111) surfaces, this suggests that oxide surfaces can in general be described by Ising or Potts models with short-range order, but not necessarily long-range order.[60] Although there have been several reports of controlling the STO surface reconstruction via control of the surface composition,[39,61] because single-crystal samples are typically prepared by quenching the sample from elevated temperatures near 1000 °C, it is likely that a glass possessing only local order is stabilized in many samples relevant for oxide thin-film growth, driven by configurational entropy.

In considering the stability of the TiO_2-DL reconstructions on real STO(001) surfaces, the role of surface adsorbates should also be considered. As shown in Figure 3, the RT5-A and RT2 reconstructions have the lowest computed surface enthalpies among the reconstructions at 1.5 TiO_2 $(1 \times 1)^{-1}$, but at this composition, the 2×1[14,16−20] and $c(4 \times 2)$[20,30,31] reconstructions have been widely reported instead. In this case, adsorbate interaction is known to play an important role. As reported by Becerra-Toledo et al.,[32,50] the experimentally observed 2×1 reconstruction is not the "dry" 2×1 structure with a high surface enthalpy as presented in Figure 3, but a hydroxylated surface stabilized by the dissociative adsorption of water. We note that the RT5-A reconstruction features similar structural motifs as those in the RT13 reconstruction. As the RT13 reconstruction does not feature a hydroxylated surface,[34,62] similar results are expected for the RT5-A reconstruction. Thus, the hydroxylated 2×1 reconstruction can be regarded as a special case for this surface composition, where the hydroxylation reduces the overall energy despite the high computed surface enthalpy of the dry structure.

Although we have presented a sequential method for generating STO(001) surface structures featuring a single structural element ($TiO_5\square$ truncated octahedron), a structural generation method based on genetic algorithm may be more appropriate to predict more complicated STO(110) and STO(111) surfaces, which feature additional tetrahedral TiO_4 structural units. Nevertheless, a similar approach could be taken to predict thermodynamically stable STO(110) and STO(111) surfaces to develop these less-utilized surfaces for oxide thin-film growth. We hypothesize that similar methods can be used to predict other surface structures.

Perhaps most significant, the approach we have used is very general and can be applied to many other systems, not just the STO surfaces, which have been the prime focus of this paper. Provided one can estimate what base structural unit will be at the surface based upon some experimental data or existing bulk inorganic chemistry, one can then construct realistic models for surfaces. This can be done relatively simply using current computation tools, and we argue will lead to significant new science.

IV. CONCLUSIONS

In summary, by using the basic TiO_6 and $TiO_5\square$ structural units that make up solved TiO_2-DL STO(001) reconstructions, we generated RT10 and RT5 STO(001) reconstructions with locally satisfied bond valence sums and predicted the thermodynamically stable reconstructions by comparing their enthalpies against the known DFT-computed convex hull. The predicted RT5 reconstruction was found to feature structural motifs that make up the RT13 reconstruction as well as several of the predicted RT10 reconstructions with lower coverages in the TiO_2 adlayer. These findings, and also a similar observation made for the previously reported RT2 and 3×3 reconstructions, indicate that the larger, more complex TiO_2-DL reconstructions with lower coverages of the TiO_2 adlayer are made up of recurrent structural motifs represented by smaller, simpler reconstructions with higher coverages of the TiO_2 adlayer. The presence of recurrent structural motifs additionally suggests that a real STO(001) surface is a glass, consisting of multiple TiO_2-DL reconstructions with short-range order, but no long-range order, although the stability of the reconstructions can be strongly influenced by adsorbate interactions, as has been previously reported for the 2×1 reconstruction. Our work outlines how thermodynamically stable TiO_2-DL STO(001) reconstructions can be predicted based on simple rules in inorganic co-ordination chemistry and physics-based energetic considerations, where a similar approach can be applied to understand the surfaces of other orientations of STO, as well as other perovskite oxides and surfaces in general.

■ ASSOCIATED CONTENT

Supporting Information

The Supporting Information is available free of charge on the ACS Publications website at DOI: 10.1021/acs.jpcc.8b07128.

Geometry of the TiO_2 double layer; details of the RT10 and RT5 TiO_2-DL structure generation; surface structures of higher-energy RT10 reconstructions; and BVS analyses (PDF)

Predicted low-energy structures (RT10-A through RT10-D and RT5-A) (ZIP)

■ AUTHOR INFORMATION

Corresponding Author

*E-mail: l-marks@northwestern.edu.

ORCID

Seyoung Cook: 0000-0001-6782-5865

Notes

The authors declare no competing financial interest.

■ ACKNOWLEDGMENTS

Work by S.C. was supported by the U.S. Department of Energy (DOE), Office of Science, Basic Energy Sciences (BES), Materials Science Division. Work by L.D.M. was supported by the DOE, Office of Science, BES, under Award #DE-FG02-01ER45945.

■ REFERENCES

(1) Mannhart, J.; Schlom, D. G. Oxide interfaces—An opportunity for electronics. *Science* **2010**, *327*, 1607−1611.

(2) Hwang, H. Y.; Iwasa, Y.; Kawasaki, M.; Keimer, B.; Nagaosa, N.; Tokura, Y. Emergent phenomena at oxide interfaces. *Nat. Mater.* **2012**, *11*, 103−113.

(3) Ohtomo, A.; Muller, D. A.; Grazul, J. L.; Hwang, H. Y. Artificial charge-modulation in atomic-scale perovskite titanate superlattices. *Nature* **2002**, *419*, 378−380.

(4) Ohtomo, A.; Hwang, H. Y. A high-mobility electron gas at the $LaAlO_3/SrTiO_3$ heterointerface. *Nature* **2004**, *427*, 423−426.

DOI: 10.1021/acs.jpcc.8b07128
J. Phys. Chem. C 2018, 122, 21991−21997

(5) Phark, S.; Chang, Y. J.; Noh, T. W. Selective growth of perovskite oxides on $SrTiO_3$ (001) by control of surface reconstructions. *Appl. Phys. Lett.* **2011**, *98*, No. 161908.
(6) Shimizu, R.; Iwaya, K.; Ohsawa, T.; Shiraki, S.; Hasegawa, T.; Hashizume, T.; Hitosugi, T. Atomic-scale visualization of initial growth of homoepitaxial $SrTiO_3$ thin film on an atomically ordered substrate. *ACS Nano* **2011**, *5*, 7967−7971.
(7) Shimizu, R.; Ohsawa, T.; Iwaya, K.; Shiraki, S.; Hitosugi, T. Epitaxial growth process of $La_{0.7}Ca_{0.3}MnO_3$ thin films on $SrTiO_3$ (001): Thickness-dependent inhomogeneity caused by excess Ti atoms. *Cryst. Growth Des.* **2014**, *14*, 1555−1560.
(8) Ohsawa, T.; Saito, M.; Hamada, I.; Shimizu, R.; Iwaya, K.; Shiraki, S.; Wang, Z.; Ikuhara, Y.; Hitosugi, T. A single-atom-thick TiO_2 nanomesh on an insulating oxide. *ACS Nano* **2015**, *9*, 8766−8772.
(9) Silly, F.; Castell, M. R. Growth of Ag icosahedral nanocrystals on a $SrTiO_3$ (001) support. *Appl. Phys. Lett.* **2005**, *87*, No. 213107.
(10) Silly, F.; Powell, A. C.; Martin, M. G.; Castell, M. R. Growth shapes of supported Pd nanocrystals on $SrTiO_3$(001). *Phys. Rev. B* **2005**, *72*, No. 165403.
(11) Enterkin, J. A.; Poeppelmeier, K. R.; Marks, L. D. Oriented catalytic platinum nanoparticles on high surface area strontium titanate nanocuboids. *Nano Lett.* **2011**, *11*, 993−997.
(12) Enterkin, J. A.; Setthapun, W.; Elam, J. W.; Christensen, S. T.; Rabuffetti, F. A.; Marks, L. D.; Stair, P. C.; Poeppelmeier, K. R.; Marshall, C. L. Propane oxidation over $Pt/SrTiO_3$ nanocuboids. *ACS Catal.* **2011**, *1*, 629−635.
(13) Martirez, J. M. P.; Kim, S.; Morales, E. H.; Diroll, B. T.; Cargnello, M.; Gordon, T. R.; Murray, C. B.; Bonnell, D. A.; Rappe, A. M. Synergistic oxygen evolving activity of a TiO_2-rich reconstructed $SrTiO_3$ (001) surface. *J. Am. Chem. Soc.* **2015**, *137*, 2939−2947.
(14) Cord, B.; Courths, R. Electronic study of $SrTiO_3$ (001) surfaces by photoemission. *Surf. Sci.* **1985**, *162*, 34−38.
(15) Andersen, J. E. T.; Møller, P. J. Impurity-induced 900 °C (2 × 2) surface reconstruction of $SrTiO_3$ (100). *Appl. Phys. Lett.* **1990**, *56*, 1847−1849.
(16) Jiang, Q.; Zegenhagen, J. $SrTiO_3$ (001) surfaces and growth of ultra-thin $GdBa_2Cu_3O_{7-x}$ films studied by LEED/AES and UHV-STM. *Surf. Sci.* **1995**, *338*, L882−L888.
(17) Castell, M. R. Scanning tunneling microscopy of reconstructions on the $SrTiO_3$ (001) surface. *Surf. Sci.* **2002**, *505*, 1−13.
(18) Naito, M.; Sato, H. Reflection high-energy electron diffraction study on the $SrTiO_3$ surface structure. *Phys. C* **1994**, *229*, 1−11.
(19) Erdman, N.; Poeppelmeier, K. R.; Asta, M.; Warschkow, O.; Ellis, D. E.; Marks, L. D. The structure and chemistry of the TiO_2-rich surface of $SrTiO_3$ (001). *Nature* **2002**, *419*, 55−58.
(20) Erdman, N.; Warschkow, O.; Asta, M.; Poeppelmeier, K. R.; Ellis, D. E.; Marks, L. D. Surface structures of $SrTiO_3$ (001): A TiO_2-rich reconstruction with a c(4 × 2) unit cell. *J. Am. Chem. Soc.* **2003**, *125*, 10050−10056.
(21) Møller, P.; Komolov, S.; Lazneva, E. Selective growth of a MgO (100)-c(2 × 2) superstructure on a $SrTiO_3$ (100)-(2 × 2) substrate. *Surf. Sci.* **1999**, *425*, 15−21.
(22) Kubo, T.; Nozoye, H. Surface structure of $SrTiO_3$ (100). *Surf. Sci.* **2003**, *542*, 177−191.
(23) Warschkow, O.; Asta, M.; Erdman, N.; Poeppelmeier, K. R.; Ellis, D. E.; Marks, L. D. TiO_2-rich reconstructions of $SrTiO_3$ (001): a theoretical study of structural patterns. *Surf. Sci.* **2004**, *573*, 446−456.
(24) Lin, Y.; Becerra-Toledo, A. E.; Silly, F.; Poeppelmeier, K. R.; Castell, M. R.; Marks, L. D. The (2 × 2) reconstructions on the $SrTiO_3$ (001) surface: A combined scanning tunneling microscopy and density functional theory study. *Surf. Sci.* **2011**, *605*, L51−L55.
(25) Tanaka, H.; Matsumoto, T.; Kawai, T.; Kawai, S. Surface structure and electronic property of reduced $SrTiO_3$ (100) surface observed by scanning tunneling microscopy/spectroscopy. *Jpn. J. Appl. Phys.* **1993**, *32*, 1405−1409.
(26) Tanaka, H.; Matsumoto, T.; Kawai, T.; Kawai, S. Interaction of oxygen vacancies with O_2 on a reduced $SrTiO_3(100)(\sqrt{5} \times \sqrt{5})$−*R*26.6° surface observed by STM. *Surf. Sci.* **1994**, *318*, 29−38.
(27) González, M. S. M.; Aguirre, M. H.; Morán, E.; Alario-Franco, M.; Perez-Dieste, V.; Avila, J.; Asensio, M. C. In situ reduction of (100) $SrTiO_3$. *Solid State Sciences* **2000**, *2*, 519−524.
(28) Newell, D. T.; Harrison, A.; Silly, F.; Castell, M. R. $SrTiO_3(001)$-$(\sqrt{5} \times \sqrt{5})$-*R*26.6° reconstruction: A surface resulting from phase separation in a reducing environment. *Phys. Rev. B* **2007**, *75*, No. 205429.
(29) Shiraki, I.; Miki, K. $SrTiO_3(100)(\sqrt{5} \times \sqrt{5})$−*R*26.6° surface observed by high-resolution scanning tunneling microscopy. *Surf. Sci.* **2011**, *605*, 1304−1307.
(30) Jiang, Q.; Zegenhagen, J. c(6 × 2) and c(4 × 2) reconstruction of $SrTiO_3$ (001). *Surf. Sci.* **1999**, *425*, 343−354.
(31) Castell, M. R. Nanostructures on the $SrTiO_3$ (001) surface studied by STM. *Surf. Sci.* **2002**, *516*, 33−42.
(32) Becerra-Toledo, A.; Castell, M.; Marks, L. Water adsorption on $SrTiO_3$ (001): I. Experimental and simulated STM. *Surf. Sci.* **2012**, *606*, 762−765.
(33) Kajdos, A. P.; Stemmer, S. Surface reconstructions in molecular beam epitaxy of $SrTiO_3$. *Appl. Phys. Lett.* **2014**, *105*, No. 191901.
(34) Kienzle, D. M.; Becerra-Toledo, A. E.; Marks, L. D. Vacant-site octahedral tilings on $SrTiO_3$ (001), the $(\sqrt{13} \times \sqrt{13})R33.7°$ surface, and related structures. *Phys. Rev. Lett.* **2011**, *106*, No. 176102.
(35) Jiang, Q.; Zegenhagen, J. $SrTiO_3$ (001)-c(6 × 2): a long-range, atomically ordered surface stable in oxygen and ambient air. *Surf. Sci.* **1996**, *367*, L42−L46.
(36) Lanier, C. H.; van de Walle, A.; Erdman, N.; Landree, E.; Warschkow, O.; Kazimirov, A.; Poeppelmeier, K. R.; Zegenhagen, J.; Asta, M.; Marks, L. D. Atomic-scale structure of the $SrTiO_3$ (001)-c(6 × 2) reconstruction: Experiments and first-principles calculations. *Phys. Rev. B* **2007**, *76*, No. 045421.
(37) Ciston, J.; Brown, H. G.; D'Alfonso, A. J.; Koirala, P.; Ophus, C.; Lin, Y.; Suzuki, Y.; Inada, H.; Zhu, Y.; Allen, L. J.; Marks, L. D. Surface determination through atomically resolved secondary electron imaging. *Nat. Commun.* **2015**, *6*, No. 7358.
(38) Silly, F.; Newell, D. T.; Castell, M. R. $SrTiO_3$ (001) reconstructions: the (2 × 2) to c(4 × 4) transition. *Surf. Sci.* **2006**, *600*, 219−223.
(39) Gerhold, S.; Wang, Z.; Schmid, M.; Diebold, U. Stoichiometry-driven switching between surface reconstructions on $SrTiO_3$ (001). *Surf. Sci.* **2014**, *621*, L1−L4.
(40) Jalan, B.; Engel-Herbert, R.; Wright, N. J.; Stemmer, S. Growth of high-quality $SrTiO_3$ films using a hybrid molecular beam epitaxy approach. *J. Vac. Sci. Technol., A* **2009**, *27*, 461−464.
(41) Kajdos, A. P.; Stemmer, S. Surface reconstructions in molecular beam epitaxy of $SrTiO_3$. *Appl. Phys. Lett.* **2014**, *105*, No. 191901.
(42) Lin, Y.; Wen, J.; Hu, L.; Kennedy, R. M.; Stair, P. C.; Poeppelmeier, K. R.; Marks, L. D. Synthesis-dependent atomic surface structures of oxide nanoparticles. *Phys. Rev. Lett.* **2013**, *111*, No. 156101.
(43) Hu, L.; Wang, C.; Kennedy, R. M.; Marks, L. D.; Poeppelmeier, K. R. The role of oleic acid: From synthesis to assembly of perovskite nanocuboid two-dimensional arrays. *Inorg. Chem.* **2015**, *54*, 740−745.
(44) Kawasaki, M.; Takahashi, K.; Maeda, T.; Tsuchiya, R.; Shinohara, M.; Ishiyama, O.; Yonezawa, T.; Yoshimoto, M.; Koinuma, H. Atomic control of the $SrTiO_3$ crystal surface. *Science* **1994**, *266*, 1540−1542.
(45) Koster, G.; Kropman, B. L.; Rijnders, G. J. H. M.; Blank, D. H. A.; Rogalla, H. Quasi-ideal strontium titanate crystal surfaces through formation of strontium hydroxide. *Appl. Phys. Lett.* **1998**, *73*, 2920−2922.
(46) Kareev, M.; Prosandeev, S.; Liu, J.; Gan, C.; Kareev, A.; Freeland, J. W.; Xiao, M.; Chakhalian, J. Atomic control and characterization of surface defect states of TiO_2 terminated $SrTiO_3$ single crystals. *Appl. Phys. Lett.* **2008**, *93*, No. 061909.
(47) Biswas, A.; Rossen, P. B.; Yang, C.-H.; Siemons, W.; Jung, M.-H.; Yang, I. K.; Ramesh, R.; Jeong, Y. H. Universal Ti-rich termination

DOI: 10.1021/acs.jpcc.8b07128
J. Phys. Chem. C 2018, 122, 21991−21997

of atomically flat $SrTiO_3$ (001), (110), and (111) surfaces. *Appl. Phys. Lett.* **2011**, *98*, No. 051904.
(48) Hatch, R. C.; Choi, M.; Posadas, A. B.; Demkov, A. A. Comparison of acid- and non-acid-based surface preparations of Nb-doped $SrTiO_3$ (001). *J. Vac. Sci. Technol., B: Nanotechnol. Microelectron.: Mater., Process., Meas., Phenom.* **2015**, *33*, No. 061204.
(49) Crosby, L. A.; Chen, B.-R.; Kennedy, R. M.; Wen, J.; Poeppelmeier, K. R.; Bedzyk, M. J.; Marks, L. D. All roads lead to TiO_2: TiO_2-rich surfaces of barium and strontium titanate prepared by hydrothermal synthesis. *Chem. Mater.* **2018**, *30*, 841−846.
(50) Becerra-Toledo, A.; Enterkin, J.; Kienzle, D.; Marks, L. Water adsorption on $SrTiO_3$ (001): II. Water, water, everywhere. *Surf. Sci.* **2012**, *606*, 791−802.
(51) Ohsawa, T.; Iwaya, K.; Shimizu, R.; Hashizume, T.; Hitosugi, T. Thickness-dependent local surface electronic structures of homoepitaxial $SrTiO_3$ thin films. *J. Appl. Phys.* **2010**, *108*, No. 073710.
(52) Enterkin, J. A.; Becerra-Toledo, A. E.; Poeppelmeier, K. R.; Marks, L. D. A chemical approach to understanding oxide surfaces. *Surf. Sci.* **2012**, *606*, 344−355.
(53) Blaha, P.; Schwarz, K.; Madsen, G.; Kvasnicka, D.; Luitz, J.; Laskowsji, R.; Tran, F.; Marks, L. D. *WIEN2k: An Augmented Plane Wave + Local Orbitals Program for Calculating Crystal Properties*; Technische Universitat Wien: Austria, 2018.
(54) Perdew, J. P.; Ruzsinszky, A.; Csonka, G. I.; Vydrov, O. A.; Scuseria, G. E.; Constantin, L. A.; Zhou, X.; Burke, K. Restoring the density-gradient expansion for exchange in solids and surfaces. *Phys. Rev. Lett.* **2008**, *100*, No. 136406.
(55) Perdew, J. P.; Ruzsinszky, A.; Csonka, G. I.; Constantin, L. A.; Sun, J. Workhorse semilocal density functional for condensed matter physics and quantum chemistry. *Phys. Rev. Lett.* **2009**, *103*, No. 026403.
(56) Hildebrandt, D.; Glasser, D. Predicting phase and chemical equilibrium using the convex hull of the Gibbs free energy. *Chem. Eng. J. Biochem. Eng. J.* **1994**, *54*, 187−197.
(57) Gibbs, J. W. *Scientific Papers: Thermodynamics*; Dover Publications: NY, 1961; Vol. *1*.
(58) Brown, I. D. Chemical and steric constraints in inorganic solids. *Acta Crystallogr., Sect. B: Struct. Sci.* **1992**, *48*, 553−572.
(59) Brown, I. D. *The Chemical Bond in Inorganic Chemistry: the Bond Valence Model*; Oxford University Press, 2002; Vol. *27*.
(60) Marks, L. D.; Chiaramonti, A. N.; Rahman, S. U.; Castell, M. R. Transition from order to configurational disorder for surface reconstructions on $SrTiO_3$ (111). *Phys. Rev. Lett.* **2015**, *114*, No. 226101.
(61) Wang, Z.; Feng, J.; Yang, Y.; Yao, Y.; Gu, L.; Yang, F.; Guo, Q.; Guo, J. Cation stoichiometry optimization of $SrTiO_3$ (110) thin films with atomic precision in homogeneous molecular beam epitaxy. *Appl. Phys. Lett.* **2012**, *100*, No. 051602.
(62) Hamada, I.; Shimizu, R.; Ohsawa, T.; Iwaya, K.; Hashizume, T.; Tsukada, M.; Akagi, K.; Hitosugi, T. Imaging the evolution of *d* states at a strontium titanate surface. *J. Am. Chem. Soc.* **2014**, *136*, 17201−17206.

DOI: 10.1021/acs.jpcc.8b07128
J. Phys. Chem. C 2018, 122, 21991−21997